

Evidence for cooper pair diffraction on the vortex lattice of superconducting niobium

A. Maisuradze,^{1,2} A. Yaouanc,^{2,3} R. Khasanov,² A. Amato,²
C. Baines,² D. Herlach,² R. Henes,⁴ P. Keppler,⁴ and H. Keller¹

¹*Physik-Institut der Universität Zürich, Winterthurerstrasse 190, CH-8057 Zürich, Switzerland*

²*Laboratory for Muon-Spin Spectroscopy, Paul Scherrer Institute, 5232 Villigen-PSI, Switzerland*

³*Institut Nanosciences et Cryogénie, SPSMS, CEA and University Joseph Fourier, F-38054 Grenoble, France*

⁴*Max-Planck-Institut für Metallforschung, Heisenbergstr. 3, D-70569 Stuttgart, Germany*

(Dated: April 7, 2019)

We investigated the Abrikosov vortex lattice (VL) of a pure Niobium single crystal with the muon spin rotation (μ SR) technique. Analysis of the μ SR data in the framework of the BCS-Gor'kov theory allowed us to determine microscopic parameters and the limitations of the theory. With decreasing temperature the field variation around the vortex cores deviates substantially from the predictions of the Ginzburg-Landau theory and adopts a pronounced conical shape. This is evidence of partial diffraction of Cooper pairs on the VL predicted by Delrieu for clean superconductors.

PACS numbers: 74.25.Uv, 74.20.Fg, 76.75.+i

The Ginzburg-Landau (GL) theory for superconductors is expressed in terms of an order parameter $\Delta(\mathbf{r})$. While the absolute value of $\Delta(\mathbf{r})$ determines the local superfluid density, its phase gradient is proportional to the local magnetic vector potential. This phase variation leads to the magnetic flux quantization and the formation of a periodic vortex lattice (VL) in type-II superconductors as was predicted by Abrikosov.¹ The VL field variation is uniquely characterized by two length scales, the magnetic penetration depth λ and the coherence length ξ_{GL} . This simple model turned out to be quite successful in describing the behavior of a superconductor in a magnetic field^{2,3} and serves as a basis for data analysis of experiments.⁴⁻⁶ However, as was shown theoretically by Delrieu,⁷ the GL model is unable to describe the magnetic response in clean superconductors at low temperatures and close to the upper critical field B_{c2} .

Soon after the publication of the microscopic Bardeen-Cooper-Schrieffer (BCS) theory for conventional superconductors,⁸ using a Green function formalism Gor'kov derived the GL equations from the BCS theory.⁹ Based on Gor'kov's equation Delrieu analyzed the field variation for classical s -wave superconductors in the vicinity of B_{c2} .⁷ He found that for clean superconductors the Cooper pairs (CPs) with ballistic trajectories through the vortex cores diffract on the periodic potential of the VL. As a result, in the low temperature limit close to B_{c2} the spatial field variation around a vortex core has a conical shape, rather than the cosine-like GL behaviour, and the fields at the minimum and saddle points are interexchanged relative to the GL prediction. Nearly at the same time Brandt came to the same conclusion based on a nonlocal theory of superconductivity.¹⁰ To observe the effect of diffraction of CPs, the carrier mean-free path ℓ_{mfp} should exceed the intervortex distance, the measurements should be done in the vicinity of $B_{c2}(T)$ such that the $\Delta(\mathbf{r})$ gradient is negligible, and the temperature should be low to minimize thermal fluctuations.

Although the theoretical study of the influence of the diffraction of CPs on the field variation was already per-

formed in 1972, it was not investigated experimentally in detail so far. Early muon spin rotation (μ SR) experiments revealed a linear high-field tail in the magnetic field distribution $D_c^{exp}(B^Z)$, in agreement with the theoretical expectation.¹¹ However, as noticed recently,¹² it occurred at an unexpectedly high temperature. As we note below the temperature stability is crucial in order to minimize experimental artifacts also leading to a linear high-field tail in $D_c^{exp}(B^Z)$. On the other hand, a μ SR study of vanadium did not reveal any deviation from the GL theory.¹³ Thus, superconductivity in the clean limit is one of the critical conditions for the observation of the high-field linear tail. Most of the novel high temperature superconductors (HTSs) are in the clean limit, and the tail should be observed provided the measurements are performed close to B_{c2} and at low temperature. Such studies of HTSs still await to be performed.

As a first superconductor to look for the effect of CP diffraction, we have chosen metallic niobium (Nb), since it is a simple BCS superconductor and pure single crystals are available. It is a type II superconductor ($\kappa \approx 0.8 > 1/\sqrt{2} \simeq 0.7$), and therefore a VL is expected in the bulk when an external field \mathbf{B}_{ext} larger than the lower critical field is applied. As shown by small angle neutron scattering, for \mathbf{B}_{ext} parallel to the crystallographic $\langle 111 \rangle$ direction the VL exhibits a simple triangular lattice.¹⁴⁻¹⁶

Our Nb sample was a single crystal disk of 13 mm diameter and 2 mm thickness with the $\langle 111 \rangle$ axis oriented normal to the disk. The samples studied here and in Ref. [11] come from the same batch, so they should be of the same metallurgical quality. The sample is further characterized when discussing its value of $B_{c2}(0)$ (see supplemental materials: Ref. [17]).

The μ SR experiments were performed at the Swiss Muon Source (S μ S), Paul Scherrer Institute (PSI), Switzerland, using the general purpose spectrometer (GPS) for $T \geq 1.6$ K and the low temperature facility (LTF) for $T \leq 1.6$ K. A field cooled procedure was used with \mathbf{B}_{ext} perpendicular to the sample plane (parallel to

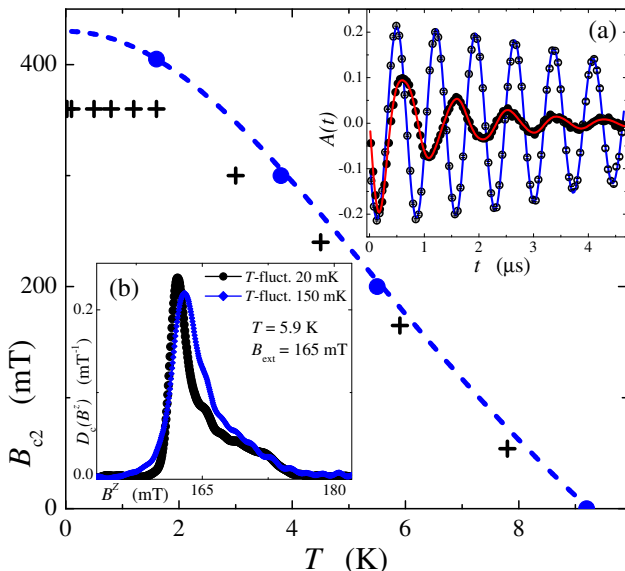


FIG. 1. (Color online) $B_{c2}(T)$ for $\mathbf{B}_{\text{ext}} \parallel \langle 111 \rangle$ as determined by μSR measurements for our Nb single crystal sample (circles). The dashed line corresponds to the equation $B_{c2}(T) = B_{c2}(0)(1 - \tau^2)/(1 + \tau^2)$ proposed in Ref. [19]. Here $\tau = T/T_{c0}$ with $T_{c0} = 9.25$ K and $B_{c2}(0) = 430(2)$ mT. The crosses indicate the points in the field-temperature diagram at which the field distributions displayed in Fig. 2 were measured. Inset (a) shows μSR asymmetry spectra $A(t)$ recorded at 1.6 K in the normal (o) and in the mixed (●) states for $B_{\text{ext}} = 450$ and 360 mT, respectively. The solid lines are fits of Eq. (1) to the data. The spectra are shown in a rotating frame of 440 and 350 mT, respectively. Inset (b) shows the effect of the sample temperature stability on $D_c^{\text{exp}}(B^Z)$. The two measurements were performed at $B_{\text{ext}} = 165$ mT and $T = 5.9$ K with different temperature regulation systems. For one of them the temperature was found to oscillate periodically around an average with a period of a few seconds and a peak to peak amplitude of 150 mK. For the other system this amplitude was reduced to about 20 mK.

the $\langle 111 \rangle$ axis). The μSR spectra were recorded in the transverse field geometry, i.e. the initial muon spin polarization \mathbf{S}_μ was perpendicular to \mathbf{B}_{ext} . By definition, \mathbf{B}_{ext} is parallel to the Z axis of the laboratory orthogonal reference frame. With this geometry the field distribution in the bulk of a superconductor can be probed $D_c^{\text{exp}}(B^Z)$.¹⁸ We explicitly distinguish $D_c(B^Z)$ from $D_c^{\text{exp}}(B^Z)$, since $D_c(B^Z)$ only stands for the distribution of a perfect VL without crystal disorder.

The forward and backward positron detectors with respect to \mathbf{S}_μ were used to build the μSR asymmetry time spectra $A(t)$ recorded with total statistics ranging from 1.0×10^7 to 8.0×10^7 positron events. Typical $A(t)$ in the normal and the superconducting states are displayed in the insert (a) of Fig. 1. Note that in contrast to the normal state, a strong damping of $A(t)$ in the superconducting state is observed which is characteristic of the local magnetic field variation due to the VL. From these

kind of measurements $B_{c2}(T)$ was determined, yielding $B_{c2}(0) = 430(2)$ mT (see Fig. 1). This value is smaller than $B_{c2}(0) = 443$ mT reported for a sample with a residual resistivity ratio $\text{RRR} = 750$.²⁰ Hence, for our sample the $\text{RRR} > 750$. Our value of $B_{c2}(0)$ indicates that the sample is of high quality and pure.²¹

As shown in the insert (b) of Fig. 1 the temperature stability is important for recording high quality data close to B_{c2} . Large fluctuations of temperature may lead to substantial smearing of the measured spectra. The experimental and theoretical field distributions presented in this letter, were obtained by Fourier transformation (FT) of the Gaussian apodized time spectra (i.e. Fourier transform of $A(t) \exp[-(t/\sigma_{\text{app}})^2/2]$ where $\sigma_{\text{app}} = 4.7 \mu\text{s}$). Note that the apodization has no influence on the analysis, since we directly fit $A(t)$, rather than $D_c^{\text{exp}}(B^Z)$.

Figure 2 displays the field distributions measured in the vicinity of $B_{c2}(T)$ from a temperature of 7.8 K close to T_{c0} (critical temperature at low field) down to 0.02 K [see Fig. 1 for the location of the points (crosses) in the field/temperature diagram]. For each $D_c^{\text{exp}}(B^Z)$ measured at LTF a relatively intense sharp peak is present at a field slightly larger than B_{ext} , in contrast to the GPS data for which only a small hump is found. This field structure (sharp peak and small hump) originates from the muons stopped in the cryostat walls and sample holder (background signal). The present GPS data are therefore of a much better quality than previous results obtained in the same temperature range showing an intense background signal.¹¹ Qualitatively, a linear high-field tail in $D_c^{\text{exp}}(B^Z)$ is inferred at maybe 1.2 K and certainly at the lower temperatures, but not at higher temperature. On the other hand, this tail is already seen at 2.6 K in the published data.^{11,18}

A μSR spectrum is described by the sum of two contributions:

$$A(t) = A_0 \cdot [F_s R_s(t) + (1 - F_s) R_{\text{bg}}(t)], \quad (1)$$

where A_0 is the total initial asymmetry and F_s the fraction of muons stopped in the sample. From analysis we determine $A_0 = 0.211(2)$ [0.217(2)] and $F_s = 0.993(2)$ [0.817(2)] for measurements carried out with the GPS [LTF] spectrometer. The function

$$R_s(t) = e^{-\frac{1}{2}\sigma_s^2 t^2} \int D_c(B^Z) \cos(\gamma_\mu B^Z t + \phi_0) dB^Z, \quad (2)$$

describes the time evolution of \mathbf{S}_μ in the sample while $R_{\text{bg}}(t) = \exp(-\sigma_{\text{bg}}^2 t^2/2) \cos(\gamma_\mu B_{\text{bg}}^Z t + \phi_0)$ accounts for the background. Here $\gamma_\mu = 851.6 \text{ Mrads}^{-1} \text{ T}^{-1}$ is the muon gyromagnetic ratio, $\sigma_{\text{bg}} \simeq 0.22(2) \mu\text{s}^{-1}$ stands for the background damping, and ϕ_0 is the initial phase. The mean field for the background B_{bg}^Z is only slightly different from B_{ext} (see Fig. 2). We write $\sigma_s^2 = \sigma_{\text{nu}}^2 + \sigma_{\text{dis}}^2$, where σ_{nu} accounts for the damping due to the nuclear ⁹³Nb spins, and σ_{dis} is the parameter describing the effect of VL disorder. As usual, we assume the effect of disorder to be modelled by a Gaussian function with a field

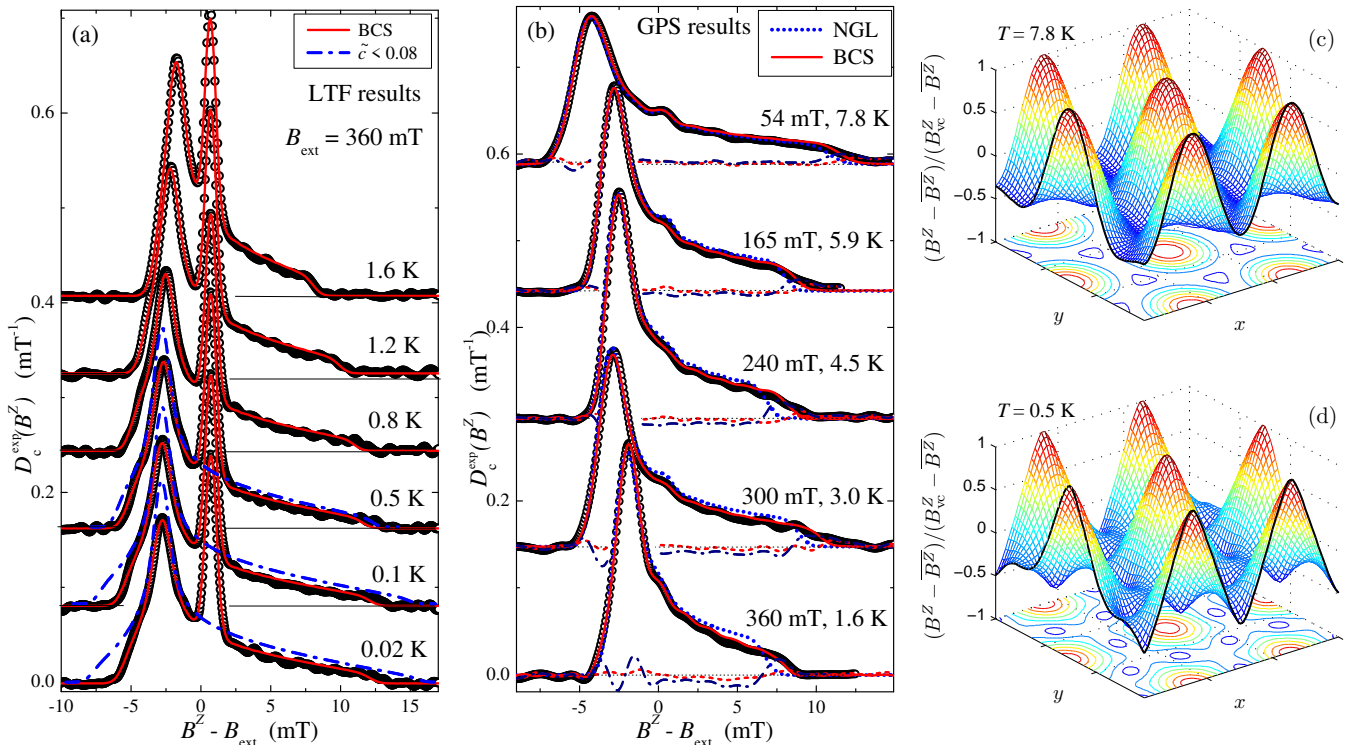


FIG. 2. (Color online) Field distributions $D_c^{\text{exp}}(B^Z)$ of Nb single crystal obtained in the vicinity of $B_{c2}(T)$ with the LTF spectrometer (a) and the GPS (b). The solid lines represent best fits of Eqs. (1)-(3) to the data. The fitting parameters are given in the Table I of Ref. [17]. Leaving the last available parameter v_F free, leads to proper fits for $T \geq 0.8$ K, but not below. The blue dashed-dotted lines in panel (a) represent the results for $T = 0.5, 0.1,$ and 0.02 K. At 0.5 K the misfits are small, but still present. The solid lines for $T \leq 0.5$ K are computed with the fixed value $\tilde{c} = 0.08$ for $T = 0.6$ K. The blue dotted lines in panel (b) correspond to fits with NGL, while the red dashed and blue dashed-dotted lines visualize the differences between $D_c^{\text{exp}}(B^Z)$ and the BCS-Gor'kov and NGL predictions, respectively. Panels (c) and (d) illustrate field variation and contour plot of $B^Z(\mathbf{r})$ obtained with BCS-Gor'kov model for the parameters at 7.8 and 0.5 K. B_{vc}^Z denotes the vortex core field.

standard deviation $\sigma_{\text{dis}}/\gamma\mu$.²² Although this is a crude approximation, we note that the influence of VL disorder on the high-field tail of $D_c^{\text{exp}}(B^Z)$ is relatively moderate compared to its effect on the low-field side.²³

We determine $D_c(B^Z)$ from the real space field map $B^Z(\mathbf{r})$ of the two-dimensional VL: $D_c(B^Z) = \int_{\text{u.c.}} \delta(B^Z(\mathbf{r}) - B^Z) d^2\mathbf{r}$, where the integral extends over the VL unit cell. In terms of its Fourier components,

$$B^Z(\mathbf{r}) = \sum_{\mathbf{K}_{m,h}} B_{\mathbf{K}_{m,h}}^Z \exp(i\mathbf{K}_{m,h} \cdot \mathbf{r}), \quad (3)$$

where the sum is over the reciprocal space.

First we analyze the data with the numerical solution of the GL (NGL) model for $B_{\mathbf{K}_{m,h}}^Z$ using Brandt's method.⁴ It only depends on λ and ξ_{GL} . The fit for the highest temperature data is reasonable (see Fig. 2b). We get $\lambda = 59.4(2)$ nm and $\sigma_s = 0.72(1)$ mT, with $\xi_{\text{GL}} = 66.5(2)$ nm estimated from the measured $B_{c2}(7.8$ K) and using the GL formula: $\xi_{\text{GL}} = (\Phi_0/2\pi B_{c2})^{1/2}$. Here, Φ_0 is the flux quantum. As expected, $\kappa = \lambda/\xi_{\text{GL}} = 0.89(1) > 1/\sqrt{2} \simeq 0.7$. The results for $T \leq 5.9$ K in Fig. 2b were

obtained with λ , ξ_{GL} , and σ_s as free parameters. The GL model fails to describe the high-field tails in $D_c^{\text{exp}}(B^Z)$. In addition, unreasonable large κ values are derived. For example: $\kappa = 48.7/28.5 = 1.7$ at 1.6 K. If κ had been taken temperature independent as it should, the misfits are even worse. As expected, the GL model can only describe $D_c^{\text{exp}}(B^Z)$ well near T_{co} .

Next we analyze the data with the BCS-Gor'kov theory.^{7,12,24} First we discuss the characteristics of $B_{\mathbf{K}_{m,h}}^Z$ in the vicinity of $B_{c2}(T)$. We use the notations of Ref. [12]. The Fourier component is a function of four parameters: $B_{\mathbf{K}_{m,h}}^Z = f_{m,h}(\tilde{a}, \tilde{b}, \tilde{c}, \tilde{d})$.^{7,12,24} Here, $\tilde{a} = -\mu_0 N_0 \Delta_0^2 \tilde{c} / 2B^Z$ does not influence the shape of $B^Z(\mathbf{r})$ and therefore $D_c(B^Z)$, but only determines the scale of the field variation. It is proportional to the density of states at the Fermi level N_0 (per spin, volume, and energy), the quantity $\Delta_0^2 = \overline{|\Delta(\mathbf{r})|^2}$ ($|\Delta(\mathbf{r})|^2$ is the spacial average of $|\Delta(\mathbf{r})|^2$), and is inversely proportional to the average field $\overline{B^Z(\mathbf{r})}$. The dimensionless parameters \tilde{b} , \tilde{c} , and \tilde{d} determine the shape of $D_c(B^Z)$ and are ex-

pressed by the ratios of four length scales: $\tilde{b} = (\Lambda/\pi\xi^B)^2$, $\tilde{c} = \Lambda/\xi^T$, and $\tilde{d} = \Lambda/\ell_{\text{mfp}}$. Here, $\Lambda = [\Phi_0/(2\pi\overline{B^Z})]^{1/2}$ is a length parameter proportional to the intervortex distance. The field and temperature dependent length scale $\xi^B = \hbar v_F/(\pi\Delta_0)$ diverges at $\overline{B^Z} \rightarrow B_{c2}$, i.e. $\tilde{b} \rightarrow 0$, while $\xi^T = \hbar v_F/(2\pi k_B T)$. The parameter \tilde{c} is strongly temperature and field dependent. It vanishes as $T \rightarrow 0$ and diverges at $T \rightarrow T_{c0}$.¹² Finally, for clean superconductors \tilde{d} is negligibly small, since ℓ_{mfp} significantly exceeds the intervortex distance.

Cooper pair diffraction may influence $D_c(B^Z)$ when three experimental conditions are met: $\Lambda \ll \ell_{\text{mfp}}$, $\Lambda \ll \pi\xi^B$, and $\Lambda \ll \xi^T$.^{7,12,24} The first condition implies a clean superconductor, the second is only satisfied in the vicinity of $B_{c2}(T)$, and the third one is only possible at low T . Thus, the minimum of $\{\ell_{\text{mfp}}, \pi\xi^B, \xi^T\}$ determines the effective diffraction length scale of CPs relative to the intervortex distance $2.693 \times \Lambda$.

The data analysis was done with $\tilde{b} \simeq 0.110(1-b)/b$ fixed ($b = \overline{B^Z}/B_{c2}(T) \simeq B_{\text{ext}}/B_{c2}(T)$).^{12,17} For Nb we get $0.01 < \tilde{b} < 0.02$, except for the spectrum at 7.8 K for which $\tilde{b} = 0.04$. Since

$$\tilde{c} = \frac{\sqrt{\Phi_0 2\pi k_B T}}{\sqrt{\overline{B^Z}} \hbar v_F} \simeq \frac{\sqrt{\Phi_0 2\pi k_B T}}{\sqrt{B_{\text{ext}}} \hbar v_F}, \quad (4)$$

the $B_{\mathbf{K}_{m,h}}^Z$ depends on \tilde{a} , \tilde{d} , v_F , T , and B_{ext} .¹⁷

The analysis of $A(t)$ for $T \geq 0.8$ K shows that $\tilde{d} \lesssim 0.01$, which agrees with the estimate of $\ell_{\text{mfp}} \simeq 7 \mu\text{m}$ for the Nb sample with RRR = 750.²⁰ Consequently, we are in the clean limit and \tilde{d} has a negligible influence on $D_c(B^Z)$. The results of the analysis are presented in Fig. 2 and Table I of Ref. [17]. The BCS-Gor'kov model describes the high-field tail significantly better at low temperatures while at the highest temperature both models reproduce the data equally well. The deviation from the GL theory and the gradual disappearance of the cut-off singularity at the maximal field is a result of the conical shape of the spatial field variation at the vortex cores (see Fig. 2d), which in turn is a consequence of the partial CP pair diffraction. This deviation cannot be explained by the presence of significant temperature and field fluctuations resulting in a large smearing parameter σ_s .²² If produced artificially the cut-off singularity in $D_c^{\text{exp}}(B^Z)$ at B_{vc}^Z vanishes as is the case in the distribution labeled 150 mK in insert (b) of Fig. 1.^{17,23} Based on the generalized Bloch equations²⁵⁻²⁷ and the analysis^{18,28} of zero-field μSR result we found that the muon diffusion²⁹⁻³¹ is negligible in the studied Nb sample (see Ref. [17]). A weak pinning¹⁷ excludes also an influence of the peak effect³²⁻³⁴ on the measured field distributions. The BCS-Gor'kov model breaks down for $T \leq 0.5$ K as shown by the dashed-dotted lines in Fig. 2a. A proper description requires to consider $B_{\mathbf{K}_{m,h}}^Z$ as a function of \tilde{a} and \tilde{c} rather than of \tilde{a} and v_F , and to keep the value of \tilde{c} at $T = 0.6$ K for the lower temperatures (solid lines in Fig. 2a).¹⁷ This means that the sharpness of the $B^Z(\mathbf{r})$ cones is limited by a physical process. Referring to Eq. (3), we suggest that

the VL structural disorder may round off the cones, as observed experimentally.

We get $v_F = 2.0(2) \times 10^5$ m/s from the fits for $T \geq 0.8$ K. This value is compatible with $v_F = 2.73 \times 10^5$ and 2.94×10^5 m/s determined from magnetization measurements.^{20,35} From the measured \tilde{a} and \tilde{c} we determine the condensation energy $E_c = -2\overline{B^Z}\tilde{a}/\mu_0\tilde{c} = 2 \times N_0\Delta_0^2/2$.^{2,36} While N_0 is a constant, Δ_0^2 is field and temperature dependent. At $T = 0$ and interpolating Δ_0^2 to zero field with a conventional formula,¹² $[-2\overline{B^Z}\tilde{a}/\mu_0\tilde{c}]/[1 - (\overline{B^Z}/B_{c2}(0))] = N_0\Delta_0^2(0)$ where $\Delta_0(0)$ is the s-wave BCS gap which is temperature independent for $T \rightarrow 0$.² From $\Delta_0(0) = 1.45$ meV (see Ref. [19]) and our estimate for the ground state $E_c(0) = N_0\Delta_0^2(0) = 2.47(9) \times 10^4 \text{ Jm}^{-3}$, we obtain $N_0 \approx 4.6 \times 10^{47} \text{ J}^{-1}\text{m}^{-3}\text{spin}^{-1} \approx 1.3 \text{ eV}^{-1}\text{atom}^{-1}\text{spin}^{-1}$. Considering the approximate nature of the linear field interpolation, these results are quite close to the specific heat result $N_0 = 0.85 \text{ eV}^{-1}\text{atom}^{-1}\text{spin}^{-1}$ (see Ref. [37]) and the GL condensation energy $B_c^2/2\mu_0 = 1.6 \times 10^4 \text{ Jm}^{-3}$ for the thermodynamic critical field $B_c = 0.20$ T.¹⁹ In our measurements all the conditions for the observation of partial CP diffraction are met at $T \lesssim 1.2$ K: $\Lambda/\pi\xi^B \leq 0.11 \ll 1$, $\Lambda/\ell_{\text{mfp}} \lesssim 0.01 \ll 1$, and $\Lambda/\xi^T = 0.16 \ll 1$.

To conclude, we investigated the magnetic field distribution for the vortex lattice (VL) of a pure Nb single crystal with the μSR technique. The data were analyzed using the solution of the BCS-Gor'kov equation proposed by Delrieu,⁷ a microscopic description in contrast to the conventional GL picture. As a result, we found strong evidence for partial Cooper pair (CP) diffraction on the periodic potential of the vortex lattice reflected in the conical narrowing of the real space field variation around the vortex cores and in the presence of a high-field linear tail in the field distribution down to 0.02 K, as expected by the BCS-Gor'kov theory. However, the BCS-Gor'kov description is only partially successful as the prediction for the low-field tail at zero-temperature limit deviates from the experimental observation, presumably due to the residual VL disorder. From the analysis we determined the Fermi velocity $v_F = 2.0(2) \times 10^5$ m/s and the ground state condensation energy $N_0\Delta_0^2(0) = 2.47(9) \times 10^4 \text{ Jm}^{-3}$ which are in reasonable agreement with literature results.^{19,20,35} The observation of partial CP diffraction should not be restricted to Nb. Under proper experimental conditions it should also be seen for any clean type-II superconductor.

This work was performed at the Swiss Muon Source (μS), Paul Scherrer Institut (PSI), Switzerland and partly supported by NCCR MaNEP sponsored by the Swiss National Science Foundation.

I. SUPPLEMENTAL MATERIALS

Abstract: Based on the phenomenological Ginzburg-Landau (GL) model and generalized Bloch equations for a diffusing magnetic probe we estimate a possible effect of the muon diffusion on the probability field distribution in Nb. We show that in the present experiments the effect of diffusion is negligibly small and cannot have any appreciable effect on the TF μ SR results given in the main text. Extremely low pinning in the studied Nb sample is demonstrated. Additional information on the data analysis is given.

A. Effect of muon diffusion on Nb μ SR spectra

As reported by Schwarz *et al.* and Wipf *et al.* in previous studies of Nb the diffusion of a light interstitial particle such as a positive muon is possible.^{29,30} As a result a muon probes the magnetic field not at a specific site in the sample but the field is averaged over a diffusion trajectory. In order to study a possible effect of muon diffusion on TF μ SR experiments presented in the main text we first determine the muon diffusion coefficient D_μ from zero field (ZF) μ SR experiment on the Nb sample studied here. Then we simulate the effect of muon diffusion on TF spectra using generalized Bloch equations for a diffusing magnetic probe.

Muon hopping rate of $\nu \sim 0.7$ MHz was determined at 2.5 K by Grasselino *et al.* from ZF μ SR experiments.³¹ In zero field the muon experiences a spin depolarization due to nuclear magnetic fields which for a static case is described with the Kubo-Toyabe function:²⁸

$$P_{\text{KT}}(t) = \frac{1}{3} + \frac{2}{3} (1 - \sigma_{\text{KT}}^2 t^2) \exp\left(-\frac{\sigma_{\text{KT}}^2 t^2}{2}\right). \quad (5)$$

The strong collision model was used in Ref. 31 for estimate of the hopping rate ν . Muon spin polarization within this model is described as follows:¹⁸

$$P_{\nu, \text{KT}}(t) = P_{\text{KT}}(t) e^{-\nu t} + \nu \int_0^t P_{\nu, \text{KT}}(t-t') P_{\text{KT}}(t') e^{-\nu t'} dt'. \quad (6)$$

The result of ZF μ SR measurement at 1.6 K is shown in Fig. 3. Time dependent asymmetry spectra are analyzed with the expression:

$$A_{\text{ZF}}(t) = A_{\text{S,ZF}} P_{\nu, \text{KT}}(t) + A_{\text{bg,ZF}} \quad (7)$$

and is shown with the solid line. The model describes the measured spectrum well. For comparison with dotted line the spectrum for $\nu = 0$ is also shown. Above, the first term describes the signal of the Nb sample while the second term is the silver background signal. Initial asymmetries are found to be $A_{\text{S,ZF}} = 0.190(1)$ and $A_{\text{bg,ZF}} = 0.020(1)$. ZF nuclear depolarization rate and muon hopping rate are $\sigma_{\text{ZF}} = 0.424(5) \mu\text{s}^{-1}$ and

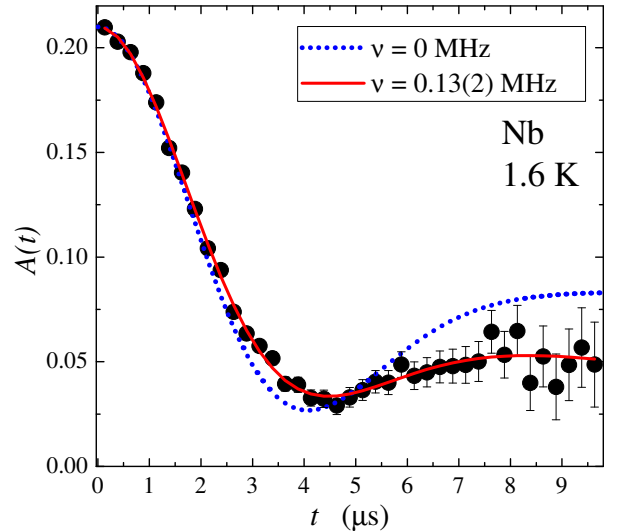


FIG. 3. (Color online) Zero field time spectrum at 1.6 K of the Nb single crystal. The solid lines are fit of the data using Eqs. (5)-(7)

$\nu = 0.13(2)$ MHz, respectively. This hopping rate is somewhat smaller than that reported in Ref. 31. However, as we can see from comparison of ZF spectra measured in the present work and that of Ref. 31, Fig. 6(a) the relaxation is indeed smaller.

The diffusion coefficient of a particle in classical statistical physics is related to its mean velocity $v = \ell\nu$ and its mean free path ℓ through the following relation:

$$D_\mu = \frac{1}{3} v \ell = \frac{1}{3} \nu \ell^2. \quad (8)$$

The lattice constant of metallic Nb and consequently the maximal distance between neighboring muon stopping sites is 0.33 nm. Therefore, for a muon hopping rate of 0.13 MHz and a mean free path of the order of lattice constant we obtain the diffusion coefficient $D_\mu = 0.0047 \text{ nm}^2 \mu\text{s}^{-1}$ at 1.6 K. This value is two orders of magnitude smaller than the TF μ SR sensitivity to muon diffusion due to the finite muon lifetime:²⁹ $1 \text{ nm}^2 \mu\text{s}^{-1}$ and it is four orders of magnitude smaller than $80(20) \text{ nm}^2 \mu\text{s}^{-1}$ reported by Schwarz *et al.*²⁹ This discrepancy can be explained by number of effects which were not considered in the analysis of the field distribution smearing around a vortex core field in Ref. 29. Namely, at present it is well established that in TF μ SR besides muon diffusion the smearing of $D_c(B^Z)$ is substantially influenced by a large number of other factors, such as: gradients and fluctuations of applied field and temperature, various kinds of vortex disorder, and nuclear fields.²² This led to a substantial overestimate of muon diffusion rate and consequently $D_\mu = 80(20) \text{ nm}^2 \mu\text{s}^{-1}$ (at 4.6 K) can be considered as the uppermost limit of a possible muon diffusion in Nb.

Next we analyze the effect of a small muon diffusion on

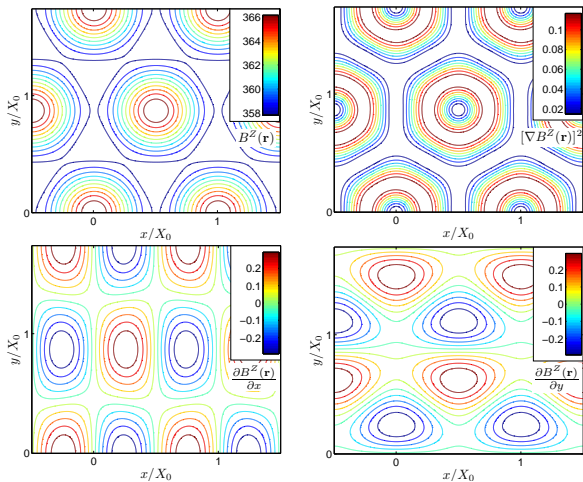


FIG. 4. (Color online) Contour plot of $B^Z(\mathbf{r})$, $[\nabla B^Z(\mathbf{r})]^2$, $\partial B^Z(\mathbf{r})/\partial x$, and $\partial B^Z(\mathbf{r})/\partial y$ obtained using the NGL model for the spectrum at 1.6 K and 360 mT ($\lambda = 48.7$ nm and $\xi = 28.5$ nm). The fields are given in units of mT while corresponding derivatives are in mT/nm and $(\text{mT}/\text{nm})^2$.

TF μ SR field distributions obtained in the main text. For a diffusing muon the complex TF muon spin polarization $\tilde{P}_{\text{TF}}^+(\mathbf{r}, t) = \tilde{P}_x(\mathbf{r}, t) + i\tilde{P}_y(\mathbf{r}, t)$ can be found from the solution of the following generalized Bloch equations:^{25,26}

$$\frac{\partial \tilde{P}_{\text{TF}}^+(\mathbf{r}, t)}{\partial t} = -\frac{\tilde{P}_{\text{TF}}^+(\mathbf{r}, t)}{T_2} - i\gamma_\mu B^Z(\mathbf{r}) + D_\mu \nabla^2 \tilde{P}_{\text{TF}}^+(\mathbf{r}, t), \quad (9)$$

Here, T_2^{-1} is the transverse muon spin relaxation rate. This rate is negligibly small, and therefore we shall suppress it. Measured TF muon spin polarization can be found as the real part of the spatially averaged complex polarization:

$$P_{\text{TF}}(t) = \text{Re} \left\{ \frac{1}{V_{\text{u.c.}}} \int_{V_{\text{u.c.}}} \tilde{P}_{\text{TF}}^+(\mathbf{r}, t) d^2\mathbf{r} \right\}. \quad (10)$$

For a small muon diffusion rate D_μ , when $\gamma_\mu D_\mu \frac{\partial^2 B^Z}{\partial k^2} t^2 \ll 1$ (here $k = x, y, \text{ or } z$) the solution of this differential equation is:^{26,27}

$$\tilde{P}_{\text{TF}}^+(\mathbf{r}, t) = P_{0,\text{TF}}^+ \exp \left[-\frac{\gamma_\mu^2 D_\mu [\nabla B^Z(\mathbf{r})]^2 t^3}{3} - i\gamma_\mu B^Z(\mathbf{r})t \right]. \quad (11)$$

Next we show that diffusion smearing cannot lead to a good description of the spectra if the NGL model is used. We simulate the influence of the muon diffusion on $D_c(B^Z)$ and compare with our measured field distribution. Only the BCS-Gor'kov model can explain the measured field distribution, in particular the high-field tail. We proceeded as follows. First the magnetic field and its gradient was computed $[B^Z(\mathbf{r}) \text{ and } \nabla B^Z(\mathbf{r})]$ using numerical solution of GL for $\lambda = 48.7$ nm and $\xi = 28.5$ nm as obtained for spectrum measured at 1.6 K and $B_{\text{ext}} = 360$ mT in the main text (see Fig. 4).

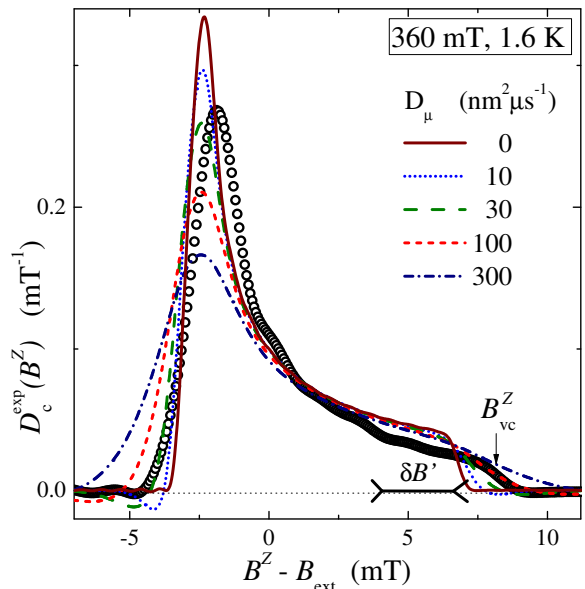


FIG. 5. (Color online) Effect of the muon diffusion on the field distribution assuming the NGL model for the vortex field distribution. Circles illustrate the experimental spectrum measured at 1.6 K and 360 mT on the GPS spectrometer. Lines result from the computation of the field distribution with the NGL model for the vortex field distribution and using Eq. 11 for the description of the muon diffusion. The figure shows that increasing the diffusion coefficient D_μ leads to a smearing of the cut-off singularities. However, none of the computed distributions looks like the measured distribution.

Then the TF muon spin polarization was computed using Eqs. (10) and (11). Finally, the field distribution was obtained by Fourier transformation of the apodized polarization function, as explained in the main text.

The results of the computations are shown in Fig. 5. In solid line we show the curve for $D_\mu = 0 \text{ nm}^2 \mu\text{s}^{-1}$. As expected the curve is not a proper description of the measured distribution. Note that this curve differs from that shown for 1.6 K in the main text, since here the Gaussian smearing originating from nuclear fields and vortex disorder is set to zero. Thus, Fig. 5 demonstrates an effect of smearing solely due to muon diffusion. With increasing D_μ smearing of the field distribution increases. But still none of the computed distribution approaches closely the measured distribution. Interestingly, a linear high-field tail is predicted at $D_\mu = 300 \text{ nm}^2 \mu\text{s}^{-1}$. However, as deduced from our zero-field measurements, it is not justified to consider large D_μ values.

Finally, we would like to stress that important is not only a linear tail but also the spectral weight of the field distribution close to B_{vc}^Z . Muon probes vortex lattice space randomly. Thus, the probability to find a muon at a distance r from the vortex core is proportional to the circular area: $P(r)dr \propto 2\pi r dr$. For $T \rightarrow 0$ and $B_{\text{ext}} \rightarrow B_{c2}$ the BCS field profile along the line crossing

two neighboring vortex cores has a sawtooth-like shape while for the NGL model it is a cosine function (see these profiles e.g. in Ref. 12). With a good approximation the field in the vicinity of the vortex core depends only on r and can be expanded in Taylor series: $B^Z(r) = B_{vc}^Z + B'r$ (for BCS) and $B^Z(r) = B_{vc}^Z + 0.5B''r^2$ (for NGL). Here, derivatives $B' < 0$ and $B'' < 0$, with $r > 0$. Inverse of these functions are:

$$r(B^Z) = \frac{\delta B^Z}{-B'} \quad \text{for BCS}$$

$$r(B^Z) = \sqrt{\frac{2\delta B^Z}{-B''}} \quad \text{for NGL.}$$

Here we denote $\delta B^Z = B_{vc}^Z - B^Z(r)$. Consequently the probability field distributions in the vicinity of a vortex core can be approximated as follows:

$$D_c^{\text{BCS}}(B^Z)dB^Z \propto -2\pi r dr = 2\pi \frac{\delta B^Z}{B'^2} dB^Z \quad \text{for BCS}$$

$$D_c^{\text{NGL}}(B^Z)dB^Z \propto -2\pi r dr = 2\pi \frac{1}{-B''} dB^Z \quad \text{for NGL.}$$

Note that above we consider that a positive dB^Z corresponds to a negative dr . Consequently the ratio of probability field distributions is $\mathcal{R} = D_c^{\text{NGL}}(B^Z)/D_c^{\text{BCS}}(B^Z) = B'^2/(-\delta B^Z B'')$. For an intervortex distance a the first derivative of the conically shaped vortex lattice $B' = -2B_{pp}/a$, while for the cosine second derivative $B'' = -4\pi^2 B_{pp}/a^2$. Here B_{pp} denotes difference between maximal and minimal fields along the line between the neighboring vortices. Therefore the ratio of spectral weights of probability field distribution in the vicinity of vortex core can be expressed as: $\mathcal{R} = B_{pp}/\pi^2 \delta B^Z$. Since $\delta B^Z \ll B_{pp}$ close to the vortex core the spectral weight of the NGL model is appreciably larger than that of the BCS model. Considering next terms in the Taylor expansion this is valid for $\delta B^Z \lesssim B_{pp}/4$. The region of the field distribution close to B_{vc}^Z is a direct fingerprint of the spatial field profile close to the vortex core. Reduction of $D_c^{\text{exp}}(B^Z)$ spectral weight in the field range marked with $\delta B'$ in Fig. 5 directly points to the narrowing of vortex core towards the conical-like shape. As can be seen a smearing does not reduce appreciably this spectral weight. Experimentally the smearing strength can be estimated from the sharpness of the cut-off in $D_c^{\text{exp}}(B^Z)$ near B_{vc}^Z (indicated by the arrow in Fig. 5). Thus, the reduction of the spectral weight in the experimental spectrum is basically determined by the field profile in the vicinity of vortex core.

B. Vortex lattice pinning

It is known that a vortex lattice may be pinned on local defects of the crystal lattice. The pinning strength substantially depends on concentration and character of pinning centers. For dirty Nb superconducting samples with

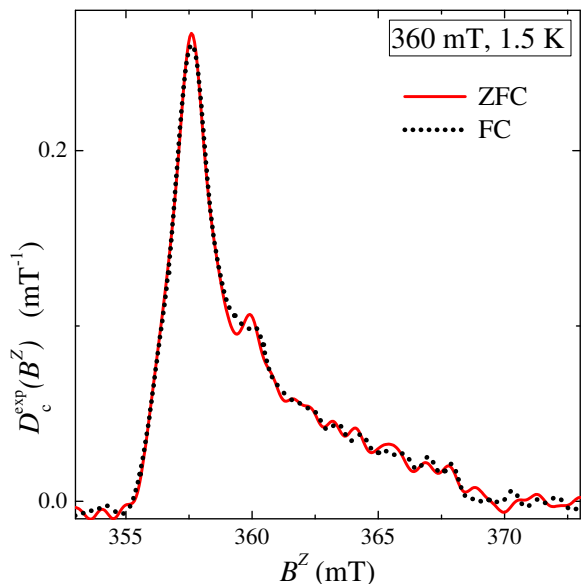


FIG. 6. (Color online) Additional test of the vortex pinning effect on $D_c^{\text{exp}}(B^Z)$ carried on the Dolly instrument at PSI. Field cooled (FC) and zero-field cooled (ZFC) experiments were performed at 1.5 K and 360 mT. These field distributions coincide within precision of the experiments which confirms the high purity of the Nb sample and its low concentration of pinning centers.

a large concentration of pinning centers and a large upper critical field ($B_{c2} \gtrsim 600$ mT) small angle neutron scattering (SANS) experiments showed a Bragg glass state with a diffraction pattern which depends on the history of applied field and temperature.³² Enhanced pinning of the vortex lattice may occur on the surface due to usually larger defect concentration at the surface of a sample.³³ These effects may be even more pronounced in the vicinity of B_{c2} due to the peak effect. In order to exclude vortex lattice distortions due to pinning and measure a sample in a condition close to thermodynamic equilibrium, a field cooling procedure is usually used. Measurements are performed after relaxation of the vortex lattice to its equilibrium state. Extreme deviation of VL from its equilibrium state may be obtained in zero field cooling (ZFC) condition. In this case the sample is cooled in zero field and afterwards a field is applied. Vortices cross the surface and travel across the sample (see e.g. Ref. 34). If there are even moderate concentration of pinning centers the VL will be far from its equilibrium state (see e.g. Ref. 5). In Fig. 6 we show ZFC and FC measurements of $D_c^{\text{exp}}(B^Z)$ for our Nb sample at the lowest temperature (1.5 K) and 360 mT carried out on the Dolly instrument at the Paul Scherrer Institute. Note that the pinning is expected to be strongest at the lowest temperatures due to the reduction of the thermal excitations of VL. Within experimental uncertainties these two field distributions coincide confirming the high purity of the

sample and its low concentration of pinning centers. This experiment demonstrates that deviations from Ginzburg-Landau predictions summarized in the main text cannot be ascribed to pinning effects in the sample.

C. Some details of analysis

As described in the main text in the clean limit a form factors and consequently a field distribution depends on the three parameters \tilde{a} , \tilde{b} , and \tilde{c} . All of them are temperature and field dependent which are determined by the temperature and field dependence of Δ_0 and temperature dependence of B_{c2} . According to Eq. (36) of Ref. 12 \tilde{b} can be expressed as follows:

$$\tilde{b} = \frac{1}{\pi^2} \frac{\xi_{\text{GL}}^2(T)}{\xi_0^2(T)} \frac{1-b}{b} \simeq 0.110 \frac{1-b}{b}. \quad (12)$$

Above, $\xi_{\text{GL}}(T) = \sqrt{\Phi_0/2\pi B_{c2}(T)}$, $\xi_0(T) = \hbar v_{\text{F}}/\pi\Delta_0(T)$, where $\xi_{\text{GL}}(0)/\xi_0(0) \simeq 1.04$ is the ratio of the Ginzburg-Landau and BCS coherence lengths (which is assumed to be temperature independent)¹² and $b = \overline{B^Z}/B_{c2}(T) \simeq B_{\text{ext}}/B_{c2}(T)$. Note that according to Eq. (E2) of Ref. 12 for $3\tilde{b} \ll 1$ there is only a weak dependence of the form factors on \tilde{b} . Temperature and field dependence of \tilde{c} are

defined as follows:

$$\tilde{c} = \frac{\Lambda}{\xi^T}. \quad (13)$$

Using the definitions $\Lambda = \sqrt{\Phi_0/(2\pi\overline{B^Z})}$ and $\xi^T = \hbar v_{\text{F}}/(2\pi k_{\text{B}}T)$ we obtain Eq. (4) of the main text. The parameter $\tilde{a} = -\mu_0 N_0 \Delta_0^2 \tilde{c} / 2\overline{B^Z}$ is related to the temperature and field dependence of Δ_0^2 . In table I we provide a summary of the fit parameters for all the data in the main text using the BCS-Gor'kov model.

D. Conclusions

To conclude, from zero-field μSR measurement we estimate the magnitude of the muon diffusion rate D_{μ} at 1.6 K in the studied Nb sample (i.e. $D_{\mu} < 0.01 \text{ nm}^2 \mu\text{s}^{-1}$). This value is found to be well below the sensitivity limit of the TF μSR experiments ($D_{\mu} = 1 \text{ nm}^2 \mu\text{s}^{-1}$, see Ref. 26) which we demonstrate by presenting the simulated TF field distributions. These simulations exclude any appreciable influence of such a low diffusion rate on the measured field distribution $D_c^{\text{exp}}(B^Z)$. Measurements of $D_c^{\text{exp}}(B^Z)$ in zero field cooled and field cooled conditions at 1.5 K and 360 mT show that the vortex lattice pinning is very small and cannot influence the deviations from the Ginzburg-Landau predictions presented in the main text. In addition, details of data analysis and further results are presented.

-
- ¹ A. A. Abrikosov, Sov. Phys. JETP **5**, 1174 (1957).
² M. Tinkham, *Introduction to Superconductivity* (McGraw-Hill, New York, 1996).
³ J. B. Ketterson and S. N. Song, *Superconductivity* (Cambridge University Press, Cambridge, 1999).
⁴ E. H. Brandt, Phys. Rev. Lett. **78**, 2208 (1997), URL <http://link.aps.org/doi/10.1103/PhysRevLett.78.2208>.
⁵ J. E. Sonier, J. H. Brewer, and R. F. Kiefl, Rev. Mod. Phys. **72**, 769 (2000), URL <http://link.aps.org/doi/10.1103/RevModPhys.72.769>.
⁶ J. E. Sonier, Reports Prog. in Phys. **70**, 1717 (2007), URL <http://iopscience.iop.org/0034-4885/70/11/R01>.
⁷ J. M. Delrieu, J. Low Temp. Phys. **6**, 197 (1972), URL <http://www.springerlink.com/content/xv12611085wj3vp6/?MUD=0&PL=1>.
⁸ J. Bardeen, L. N. Cooper, and J. R. Schrieffer, Phys. Rev. **108**, 1175 (1957), URL <http://link.aps.org/doi/10.1103/PhysRev.108.1175>.
⁹ L. Gor'kov, Sov. Phys. JETP **36**, 1364 (1959).
¹⁰ E. H. Brandt, Phys. Stat. Sol. B **64**, 467 (1974), ISSN 1521-3951, URL <http://dx.doi.org/10.1002/pssb.2220640207>.
¹¹ D. Herlach, G. Majer, J. Major, J. Rosenkranz, M. Schmolz, W. Schwarz, A. Seeger, W. Templ, E. Brandt, U.Essmann, et al., Hyperfine Interactions **63**, 41 (1990), URL <http://www.springerlink.com/content/?k=pub%3a%28Hyperfine+interactions%29+vol%3a%2863%29+P%3a%2841%29>.
¹² A. Maisuradze and A. Yaouancq, Phys. Rev. B **87**, 134508 (2013), URL <http://link.aps.org/doi/10.1103/PhysRevB.87.134508>.

TABLE I. Summary of the fit parameters using the BCS-Gor'kov model [Eqs. (1)-(3) of the main text] for the data presented in the main text. Note that the parameter \tilde{b} was fixed according to Eq. (12) while \tilde{c} was determined with Eq. (13) (e.g. leaving common v_{F} free for all the spectra). The error in the temperature includes the magnitude of the temperature fluctuations.

T (K)	B_{ext} (mT)	\tilde{a} (mT)	\tilde{b}	\tilde{c}	\tilde{d}	σ_s (mT)
0.020(1)	360	0.623(1)	0.021	0.08	0.01	0.44(1)
0.100(1)	360	0.623(3)	0.021	0.08	0.01	0.57(2)
0.500(1)	360	0.599(4)	0.021	0.08	0.01	0.43(1)
0.800(1)	360	0.770(5)	0.019	0.105(11)	0.01	0.39(1)
1.200(1)	360	1.135(8)	0.017	0.157(16)	0.01	0.38(1)
1.600(1)	360	1.328(8)	0.014	0.201(20)	0.01	0.34(1)
3.00(15)	300	4.56(3)	0.018	0.396(40)	0.01	0.49(1)
4.50(2)	240	7.07(5)	0.012	0.590(60)	0.01	0.48(1)
5.90(2)	165	12.6(1)	0.011	0.776(80)	0.01	0.58(1)
7.80(2)	54	115(1)	0.038	1.75(18)	0.01	0.60(1)

- <http://link.aps.org/doi/10.1103/PhysRevB.87.134508>.
- ¹³ M. Laulajainen, F. D. Callaghan, C. V. Kaiser, and J. E. Sonier, *Phys. Rev. B* **74**, 054511 (2006), URL <http://link.aps.org/doi/10.1103/PhysRevB.74.054511>.
- ¹⁴ J. Schelten, H. Ullmaier, and W. Schmatz, *physica status solidi (b)* **48**, 619 (1971), ISSN 1521-3951, URL <http://dx.doi.org/10.1002/pssb.2220480219>.
- ¹⁵ R. Kahn and G. Parette, *Solid State Commun.* **13**, 1839 (1973), ISSN 0038-1098, URL <http://www.sciencedirect.com/science/article/pii/0038109873907412>.
- ¹⁶ S. Mühlbauer, C. Pfleiderer, P. Böni, M. Laver, E. M. Forgan, D. Fort, U. Keiderling, and G. Behr, *Phys. Rev. Lett.* **102**, 136408 (2009), URL <http://link.aps.org/doi/10.1103/PhysRevLett.102.136408>.
- ¹⁷ In supplemental materials we determine the muon diffusion rate in the studied Nb sample and estimate its possible effect on a field distribution. We provide also additional details on the analysis and demonstrate an extremely low pinning.
- ¹⁸ A. Yaouanc and P. Dalmas de Réotier, *Muon Spin Rotation, Relaxation, and Resonance: Applications to Condensed Matter*, International Series of Monographs on Physics 147 (Oxford University Press, Oxford, 2011).
- ¹⁹ D. K. Finnemore, T. F. Stromberg, and C. A. Swenson, *Phys. Rev.* **149**, 231 (1966), URL <http://link.aps.org/doi/10.1103/PhysRev.149.231>.
- ²⁰ S. J. Williamson, *Phys. Rev. B* **2**, 3545 (1970), URL <http://link.aps.org/doi/10.1103/PhysRevB.2.3545>.
- ²¹ N. Y. Alekseyevskiy, V. I. Nizhankovskiy, and H.-H. Berthel, *Fiz. Met. Metalloved.* **37**, 63 (1974).
- ²² E. H. Brandt, *J. Low Temp. Phys.* **73**, 355 (1988), URL <http://www.springerlink.com/content/p8442442n7486186/?MUSE=1>.
- ²³ A. Maisuradze, R. Khasanov, A. Shengelaya, and H. Keller, *J. Phys.: Condens. Matter* **21**, 075701 (2009), URL <http://stacks.iop.org/0953-8984/21/i=7/a=075701>.
- ²⁴ J. M. Delrieu, Ph.D. thesis, University of Paris-Orsay (1974).
- ²⁵ H. C. Torrey, *Phys. Rev.* **104**, 563 (1956), URL <http://link.aps.org/doi/10.1103/PhysRev.104.563>.
- ²⁶ A. Seeger, *Phys. Lett. A* **74**, 259 (1979), ISSN 0375-9601, URL <http://www.sciencedirect.com/science/article/pii/03759601>.
- ²⁷ C. P. Slichter, *Principles of Magnetic Resonance* (Springer, Berlin, 1996), third enlarged and updated edition.
- ²⁸ T. Yamazaki, *Hyperfine Interactions* **104**, 3 (1997), ISSN 0304-3843, URL <http://dx.doi.org/10.1023/A:3A1012696615710>.
- ²⁹ W. Schwarz, E. H. Brandt, K.-P. Doring, U. Esmann, K. Furderer, M. Gladisch, D. Herlach, G. Majer, H.-J. Munding, H. Orth, et al., *Interactions* **31**, 247 (1986), URL <http://link.springer.com/content/pdf/10.1007%2FBF02401567>.
- ³⁰ H. Wipf, D. Steinbinder, K. Neumaier, P. Gutsmedl, A. Magerl, and A. J. Dianoux, *EPL (Europhysics Letters)* **4**, 1379 (1987), URL <http://stacks.iop.org/0295-5075/4/i=12/a=007>.
- ³¹ A. Grassellino, C. Beard, P. Kolb, R. Laxdal, N. S. Lockyer, D. Longuevergne, and J. E. Sonier, *Phys. Rev. ST Accel. Beams* **16**, 062002 (2013), URL <http://link.aps.org/doi/10.1103/PhysRevSTAB.16.062002>.
- ³² N. D. Daniilidis, S. R. Park, I. K. Dimitrov, J. W. Lynn, and X. S. Ling, *Phys. Rev. Lett.* **99**, 147007 (2007), URL <http://link.aps.org/doi/10.1103/PhysRevLett.99.147007>.
- ³³ H. A. Hanson, X. Wang, I. K. Dimitrov, J. Shi, X. S. Ling, B. B. Maranville, C. F. Majkrzak, M. Laver, U. Keiderling, and M. Russina, *Phys. Rev. B* **84**, 014506 (2011), URL <http://link.aps.org/doi/10.1103/PhysRevB.84.014506>.
- ³⁴ A. J. Qviller, V. V. Yurchenko, Y. M. Galperin, J. I. Vestgård, P. B. Mozhaev, J. B. Hansen, and T. H. Johansen, *Phys. Rev. X* **2**, 011007 (2012), URL <http://link.aps.org/doi/10.1103/PhysRevX.2.011007>.
- ³⁵ H. R. Kerchner, D. K. Christen, and S. T. Selmla, *Phys. Rev. B* **24**, 1200 (1981), URL <http://link.aps.org/doi/10.1103/PhysRevB.24.1200>.
- ³⁶ Here, factor of 2 considers integration over spin degrees of freedom.
- ³⁷ A. Junod, J.-L. Jorda, and J. Muller, *Journal of Low Temperature Physics* **62**, 301 (1986), ISSN 0022-2291, URL <http://dx.doi.org/10.1007/BF00683466>.